Dynamic Instability in Intergranular Fracture

V. Yamakov,[1,*] E. Saether,[2] D. R. Phillips,[3] and E. H. Glaessgen[2]
[1]National Institute of Aerospace, Hampton, Virginia 23666, USA
[2]NASA Langley Research Center, Hampton, Virginia 23681, USA
[3]Lockheed Martin Space Operations, Hampton, Virginia 23681, USA
(Received 21 March 2005; published 30 June 2005)

A molecular-dynamics model for crack propagation under steady-state conditions is used to study dynamic instabilities along a grain boundary in aluminum that occur when the crack speed approaches $1/3$ of the material's Rayleigh wave speed. Instead of crack branching, as is characteristic for a crack propagating in a homogeneous environment, the instability of an intergranular crack results in a periodic series of dislocation bursts. These bursts limit the crack speed and produce velocity oscillations with a large increase in energy dissipation that increases the grain boundary toughness.

DOI: 10.1103/PhysRevLett.95.015502 PACS numbers: 62.20.Mk, 68.35.−p

Recently, considerable attention has been given to the dynamic instabilities that occur during fracture. In homogeneous media at speeds greater than $1/3$ of the Rayleigh wave speed c_R, these instabilities result in crack branching and roughness at the crack surface, dramatically increasing the crack area and the energy dissipation at the crack tip [1–4]. In ductile polycrystals, such as fcc metals, the *transgranular* crack propagation, taking place through the grains, experiences a ''dynamic brittle-to-ductile transition'' as a result of the dynamic instability [2,5]. The transition is associated with blunting of an initially brittle crack in an explosion of dislocations at the crack tip [2,5], together with crack branching along the available slip planes and surface roughening [6]. This mechanism increases the material toughness several times when compared to brittle fracture, occurring, for example, at cryogenic temperatures [7]. In *intergranular* fracture, in which cracks propagate along the grain boundary (GB), the crack tip is channeled by the weaker GB layer. Of particular interest is how this constrained condition affects the crack dynamics and the instability in the crack motion, compared to transgranular fracture [1–6].

In this work, a molecular-dynamics (MD) simulation model for crack propagation under steady-state conditions and low temperature (100 K) is used to study dynamic instability in the propagation of a crack through a flat GB in Al (modeled by the interatomic potential of Mishin *et al.* [8]). The configuration is based on a well-studied analytical model for steady-state crack propagation [9,10]. The model represents a laterally strained strip of elastic material. The strip is infinite in the longitudinal direction, and a semi-infinite crack propagates through it [9]. Far ahead of the crack tip, the strip is under uniform tension. Far behind the tip, the tension is relieved and the crack opening becomes constant. Thus, there are two stable states for the material: ''closed,'' in front of the crack tip, and ''open,'' behind the crack tip. The crack propagation is a continuous steady-state transition between these two states [9]. Applying this model as a base for the MD simulation ensures that after some initial growth, the crack propagation proceeds under steady-state conditions independent of the crack length.

The following MD simulation setup, shown in Fig. 1, is used. With periodic boundary conditions in all directions, the model represents a multilayer system of alternating sets of thick and thin crystalline layers separated by four flat GBs. The two broad layers, marked as ''Crystal I'' and ''Crystal II'' form a bicrystalline system with a flat GB in the middle, through which the crack propagates. The two smaller layers serve as shock-wave absorbers, where a damping friction coefficient is applied to the atoms to absorb the phonon waves generated from the crack tips [11]. In addition, the GBs formed by these layers act as absorbers for dislocations that may be emitted from the crack during propagation. The normal to the strip (z direction) for all layers is along the $[1\ 1\ 0]$ crystallographic axis. The layers are misoriented symmetrically to one another at an angle of 89.42°. The four GBs formed are $\langle 110\rangle\ \Sigma 99$ symmetric tilt GBs, for which the atomic structure in Al is known from the literature [12]. This GB is of a high-angle type with a quasiperiodic structure and large excess (i.e.,

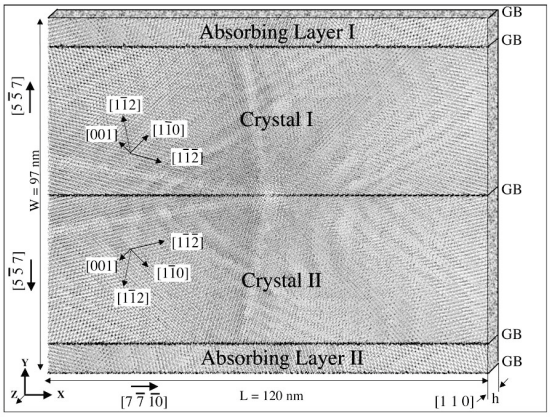

FIG. 1. Atomistic snapshot giving the crystallography and structure of the MD system. See text for details.

above the perfect crystal) energy, $\gamma_{GB} = 0.65 \pm 0.05$ J/m^2, which facilitates its decohesion [13]. The surface energy of the {5 5 7} GB plane is estimated at $\gamma_s = 0.952 \pm 0.0005$ J/m^2. Both, γ_{GB} and γ_s, are estimated for a relaxed structure at 100 K. The strip thickness h in the z direction (Fig. 1) is limited to 10{2 2 0} atomic layers or $h = 2.9$ nm. This thickness is large enough to prevent interference of the atoms with their periodic images, and to preserve the local 3D physics in the system. Because of the small thickness, the system size in the x and y directions extends up to 120 and 97 nm, respectively, while the number of simulated atoms is limited to 1 994 000 allowing for the simulation to be carried out on a modest Beowulf cluster. In addition, the ⟨110⟩ texture makes two of the four {1 1 1} slip planes in the fcc lattice (along the two ⟨112⟩ directions in Fig. 1) available for dislocation glide and cross-slip events, as in a fully 3D space [14].

The simulated system is prestrained by applying constant external hydrostatic load ($\sigma_{xx} = \sigma_{yy} = \sigma_{zz} = 4.25$ GPa) at a constant temperature of 100 K using the Parrinello-Rahman constant-stress technique combined with the Nose-Hoover thermostat [15]. After reaching mechanical equilibrium at $\varepsilon_{xx} = \varepsilon_{yy} = \varepsilon_{zz} = 1.78\%$ strain, the system size is fixed. The hydrostatic loading helps to eliminate plasticity effects not related to the crack, like spontaneous dislocation nucleation from the GBs [14], which could otherwise dominate the deformation.

The identification of different structural formations in the system is performed continuously during the simulation by applying the common neighbor analysis (CNA) technique [16]. CNA is used to identify atoms in three states: fcc state—representing the perfect crystal lattice; hcp state—representing stacking faults and twin boundaries; and disordered state (non-fcc and non-hcp atoms)—representing GB layer and dislocation cores. In addition, atoms that have lost more than 1/3 of their neighbors in the interaction range are considered as surface atoms. On average, 1 nm^2 of a flat {5 5 7} surface contains 16 surface atoms, which is used to estimate the crack free surface S, and, when divided by $2h$, gives an effective crack length l.

The crack is initiated by screening the interatomic potential between atoms at both sides of the GB plane between Crystal I and Crystal II (Fig. 1) along a region of length $l_0 = a_0[7\ 7\ 10] = 5.7$ nm (for the potential used, $a_0 = 0.405$ nm [8]). The crack starts growing if l_0 is larger than the critical Griffith length L_g (defined when the energy spent to create the upper and lower crack surfaces $2\gamma_s$ minus the energy gained by destroying the GB, γ_{GB}, is equal to the released strain energy per length l, i.e., $2\gamma_s - \gamma_{GB} = -dU/dl$). By calculating dU/dl as a function of σ and l, L_g is estimated to be 4.21 nm. This calculation is performed using anisotropic finite-element (FE) simulations on the elastic equivalent of the MD system. The displacements corresponding to hydrostatic strain are applied to a configuration that is discretized with generalized plane strain elements in the ABAQUS commercial software package [17]. The FE calculations show that dU/dl becomes nearly constant at $l > 30$ nm (as is shown later), implying a steady-state propagation above this crack length.

Nine MD simulation snapshots of the crack propagation are shown in Fig. 2. The first two [Figs. 2(a) and 2(b)], made shortly after the crack initiation, reveal that both crack tips start propagating in a ductile manner, emitting a series of dislocations and deformation twins. The twinning, which is not unusual in crack propagation in Al [18], is more active at the tip propagating in the $-x$ direction in Fig. 2(a) than for the tip propagating in the $+x$ direction. The difference is due to the orientation of the {1 1 1} slip planes relative to the GB plane. The Rice criterion for dislocation emission vs cleavage at a crack tip [19] shows that this orientation makes the dislocation emission and twinning more favorable for propagation in the $-x$ direction, and decohesion of the GB more favorable in the $+x$ direction. The subsequent discussion focuses on the propagation in the $+x$ direction [Figs. 2(c)–2(f)], where dynamic instability occurs.

Although the crack propagation in the $+x$ direction is expected to be brittle, the snapshots in Fig. 2 show that dislocations are emitted in this direction. A careful observation of the snapshots in Figs. 2(c)–2(h) reveals a certain

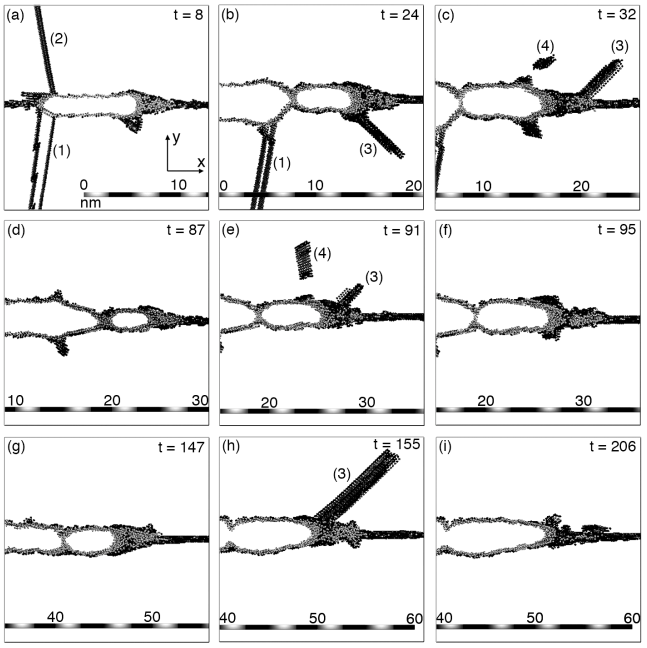

FIG. 2. A series of snapshots taken at various times t from the crack initiation given in ps. Four types of atoms are identified (see text): fcc, hcp, disordered, and surface atoms. Only the non-fcc atoms are shown. The surface atoms are shown in gray, while hcp and disordered atoms are shown in black. Thus, the straight lines of black atoms away from the crack are either twin boundaries (1) or stacking faults (2) in a partial (3) or perfect (4) dislocation.

pattern. Rather than being continuous, after the initial 30 ps, the dislocation emission becomes intermittent and forms dislocation bursts at about every 60 ps [see Figs. 2(c), 2(e), and 2(h) at $t = 32$, 91, and 155 ps, respectively]. During the time between these bursts, the crack propagates substantially by cleavage [Figs. 2(d), 2(f), 2(g), and 2(i)]. The cleavage occurs through the nucleation of microvoids ahead of the crack tip and their subsequent joining with the crack, as reported in [6] for the NiAl alloy. Figure 3(a) shows that the dislocation emissions correlate very well with the peaks in energy density Φ at the crack tip. Figure 3(b) shows a similar correlation with the speed of crack growth ν, which oscillates between zero and $0.4c_R$ with the period of the dislocation bursts seen in Fig. 2. The dislocation bursts occur shortly after the velocity peaks at the critical value $\nu_c = 0.35c_R$ when the crack propagation becomes unstable. The peaks in Φ, appearing shortly after ν approaches ν_c, indicate increased energy storage at the crack tip at $\nu = \nu_c$ in the form of a shock wave, since the energy from the crack tip can be released only at the Rayleigh speed. It is possible that this high-energy density enables dislocation bursts and dissipates through them.

On several occasions in Fig. 3(b), a negative crack growth is calculated. This result is due to a reduction in the surface area used to estimate l. Relaxation processes, such as smoothing out the free surface after microvoids coalescence during crack growth, together with the appearance of local healing at the crack tips, give an effective shortening of the crack.

A comparison between the stored potential energy of the MD system with the stored elastic energy from continuum elastic FE simulations on a statically equivalent system of the same domain (Fig. 4) shows that there is more energy release in the MD simulation than can be accounted for by continuous elastic processes alone. The FE curve in Fig. 4 shows a constant energy decrease for $l > 30$ nm, implying a steady-state propagation. Over most of the crack growth, the MD potential energy is proportional to the FE energy. On three occasions, though, at $l = 30$, 45, and 60 nm, which coincide with the periodic dislocation bursts, the MD energy decreases abruptly, indicating an increased energy release due to plastic processes that are not accounted for in the elastic FE model. At $l = 60$ nm (see Fig. 4), the last dislocation burst [Fig. 2(h)] exhausts a sufficient portion of the remaining energy in the finite MD system, and the crack is arrested.

While dynamic instability in crack propagation is a well known phenomenon, it has always been associated with branching of the crack tip or roughening of the crack surface accompanied by a strong emission of dislocations [1–6]. This study shows that in the case of an intergranular crack propagating along a weak interface (a high-energy GB in this case), branching or roughening may not appear. Nevertheless, the dynamic instability still occurs, as predicted for this model [10], but it reveals itself through a series of dislocation bursts until the crack is finally arrested. Because of the lack of branching, the crack tip preserves its initial sharpness (see Fig. 2). Thus, after the velocity reduces, and the dislocation burst ceases, the crack may resume its propagation until the velocity increases to produce the next instability.

The estimated value $\nu_c = 0.35c_R$, at which the dislocation bursts are initiated, agrees with $0.32c_R$, found in the MD simulations of Abraham *et al.* [1], and also with the theoretical estimate of $0.4c_R$, given by Gao [3]. The dependence of ν_c on the width of the strip, as predicted in [10], has not been studied, but there is good agreement for the case of a thin strip [$\nu_c \approx (0.3–0.4)c_R$] [10].

In the presented MD simulation study, dynamic instability is found to occur during fracture along a high-angle GB in Al. This instability is shown to create a series of periodic dislocation bursts, while preserving a sharp crack tip. During instability, the GB interface prevents branching or roughening of the crack surface, making it possible for

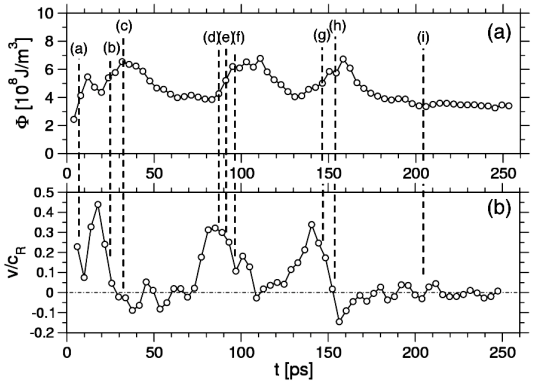

FIG. 3. (a) Energy density Φ around the crack tip vs time—Φ is the sum of potential and kinetic energy taken over a volume of $[5\ 5\ 7]a_0 \times [7\ 7\ 10]a_0 \times h = 66$ nm^3 around the crack tip. (b) The speed of crack growth in units of the Rayleigh wave speed $c_R = 3180$ m/s for this model. The letters (a) through (i) relate to the snapshots in Fig. 2.

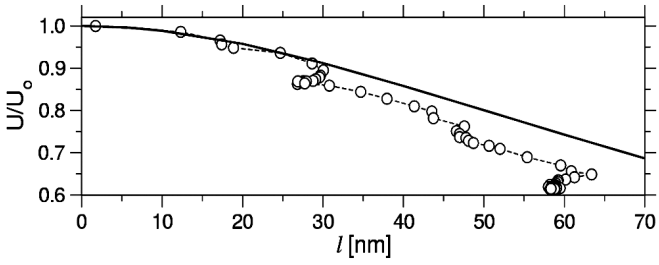

FIG. 4. Stored potential energy vs increasing crack length. Open circles relate to the potential energy of the MD system (excluding the surface and GB energy), and the solid line relates to the elastic energy of the FE system. As the FE system is more idealized by not including the GB elastic zone and having no GB and surface energies, the data are normalized by the energies of the two systems with no crack for a better comparison.

the crack to restore its growth when the propagation speed decreases well below ν_c. This mechanism suggests that crack blunting may not occur as readily during intergranular fracture as it does during transgranular fracture.

V. Yamakov and D. R. Phillips were sponsored through cooperative agreement NCC-1-02043 with the National Institute of Aerospace and Contract No. NAS1-00135 with Lockheed Martin Space Operations, respectively.

*Corresponding author.
Electronic address: yamakov@nianet.org

[1] F. F. Abraham *et al.*, Phys. Rev. Lett. **73**, 272 (1994).
[2] F. F. Abraham, J. Mech. Phys. Solids **49**, 2095 (2001).
[3] H. Gao, J. Mech. Phys. Solids **44**, 1453 (1996).
[4] E. Sharon, S. P. Gross, and J. Fineberg, Phys. Rev. Lett. **74**, 5096 (1995).
[5] S. J. Zhou *et al.*, Phys. Rev. Lett. **78**, 479 (1997).
[6] D. Farkas, Philos. Mag. A **80**, 1425 (2000).
[7] A. Rossoll, C. Berdin, and C. Prioul, Int. J. Fract. **115**, 205 (2002).
[8] Y. Mishin *et al.*, Phys. Rev. B **59**, 3393 (1999).
[9] M. Barber, J. Donley, and J. S. Langer, Phys. Rev. A **40**, 366 (1989).
[10] E. S. C. Ching, Phys. Rev. E **49**, 3382 (1994).
[11] P. Gumbsch, S. J. Zhou, and B. L. Holian, Phys. Rev. B **55**, 3445 (1997).
[12] U. Dahmen *et al.*, Philos. Mag. Lett. **62**, 327 (1990).
[13] D. Wolf, J. Mater. Res. **5**, 1708 (1990).
[14] V. Yamakov *et al.*, Nat. Mater. **1**, 45 (2002).
[15] S. Melchionna, G. Ciccotti, and B. L. Holian, Mol. Phys. **78**, 533 (1993).
[16] A. S. Clarke and H. Jonsson, Phys. Rev. E **47**, 3975 (1993).
[17] D. Hibbitt, B. Karlsson, and P. Sorensen, *ABAQUS/Standard User's Manual* (Hibbitt, Karlsson, and Sorensen, Inc., Providence, RI, 2004).
[18] S. Hai and E. B. Tadmor, Acta Mater. **51**, 117 (2003).
[19] J. R. Rice, J. Mech. Phys. Solids **40**, 239 (1992).